
Article:
Gedalin, M. orcid.org/0000-0003-1236-4787, Golan, M., Vink, J. orcid.org/0000-0002-4708-4219 et al. (2 more authors) (2023) Electron heating in shocks: statistics and comparison. Journal of Geophysical Research: Space Physics, 128 (9). e2023JA031627. ISSN 2169-9380

https://doi.org/10.1029/2023ja031627

JGR Space Physics

RESEARCH ARTICLE
10.1029/2023JA031627

Electron Heating in Shocks: Statistics and Comparison

Michael Gedalin[1], Michal Golan[1], Jacco Vink[2], Natalia Ganushkina[3,4], and Michael Balikhin[5]

[1]Department of Physics, Ben-Gurion University of the Negev, Beer-Sheva, Israel, [2]University of Amsterdam, Amsterdam, The Netherlands, [3]Finnish Meteorological Institute, Helsinki, Finland, [4]Climate and Space Science and Engineering Department, University of Michigan, Ann Arbor, MI, USA, [5]University of Sheffield, Sheffield, UK

Key Points:

- At high Mach numbers electron heating stabilizes at ∼2%–5% of the incident ion energy
- Electron temperature in the far downstream region is lower than at the overshoot
- The ratio of the downstream electron-to-ion temperatures stabilizes at about 0.1–0.15

Correspondence to:

M. Gedalin,
gedalin@bgu.ac.il

Citation:

Gedalin, M., Golan, M., Vink, J., Ganushkina, N., & Balikhin, M. (2023). Electron heating in shocks: Statistics and comparison. *Journal of Geophysical Research: Space Physics*, *128*, e2023JA031627. https://doi.org/10.1029/2023JA031627

Received 21 APR 2023
Accepted 30 AUG 2023

Author Contributions:

Conceptualization: Michael Gedalin
Formal analysis: Michael Gedalin, Michal Golan
Funding acquisition: Michael Gedalin, Jacco Vink, Natalia Ganushkina, Michael Balikhin
Investigation: Michael Gedalin, Michal Golan, Natalia Ganushkina, Michael Balikhin
Methodology: Michael Gedalin, Michal Golan, Jacco Vink, Michael Balikhin
Validation: Michael Gedalin, Jacco Vink
Visualization: Michael Gedalin
Writing – original draft: Michael Gedalin
Writing – review & editing: Michael Gedalin, Michal Golan, Jacco Vink, Natalia Ganushkina, Michael Balikhin

Abstract Supernova remnant (SNR) shocks are the highest Mach number non-relativistic shocks in electron-ion plasmas. These shocks are the most efficient particle accelerators in space. SNR shock parameters are inferred from measurements of electromagnetic radiation from heated and accelerated particles. Temperature of the shock heated electrons is one of the most important parameters in supernova remnant shocks. Knowledge of the downstream electron-to-ion temperature ratio or of the ratio of the downstream electron temperature to the incident ion energy is crucial for understanding physics of the very high-Mach number SNR shocks. Heliospheric shocks have substantially lower Mach numbers than SNR shocks but can be extensively studied in in situ observations with further extrapolation of the findings to higher Mach numbers. Magnetospheric Multiscale mission observations of the Earth bow shock are used to analyze dependence of the electron heating on the shock Mach number. It is found that the ratio of the downstream electron temperature to the incident ion energy decreases with the increase of the Mach number. At high Mach numbers this ratio and stabilizes at about 2.5%. The electron-to-ion temperature ratio stabilizes at about 10%. The peak electron temperature occurs at the overshoot maximum, further downstream electrons cool down. The mean ratio of the 4.5 s averages of the downstream and maximum electron temperatures is 0.85. Electron heating does not follow the thermodynamic adiabatic law. The heating and cooling behavior implies that the energy is provided by the overall cross-shock potential while small-scale electric fields rapidly isotropize the electron distribution.

1. Introduction

Supernova remnant (SNR) shocks are the highest Mach number non-relativistic shocks in plasmas composed mainly of protons and electrons. It is widely believed that these collisionless shocks are the most efficient particle accelerators in space. SNR shocks cannot be studied with in situ observations. The parameters, crucial for understanding physics of these shocks, are inferred from measurements of electromagnetic radiation from heated and accelerated particles. On the other hand, heliospheric shocks can be extensively studied with in situ measurements. The Mach number, which is the ratio of the normal component of the upstream plasma velocity in the shock frame (or, equivalently, the shock speed in the plasma frame) V_u to the speed of the corresponding mode, is the main shock parameter. Fast shocks are in the focus of the present study, so that the fast Mach number $M_F = V_u/v_F$ is relevant for the discussion. Here v_F is the fast magnetosonic speed (see Section 3). The Mach numbers of SNR shocks may be as large as 10^2–10^3 (Vink, 2020). For heliospheric shocks the highest Mach numbers $\sim 10^2$ are observed at Saturn (Sulaiman et al., 2015). The most detailed investigated Earth bow shock has typical Mach numbers of ∼10 (Lalti et al., 2022). Although the Mach numbers of heliospheric shocks are substantially lower than that of SNR shocks, the results of the analysis of heliospheric shocks may be extrapolated to higher Mach numbers in the assumption that the laws of collisionless shock physics are the same. In addition, it is possible that a cosmic-ray precursor results in effective decrease of the Mach number of SNR shocks (Bell, 2004, 2005).

Knowledge of the downstream electron-to-ion temperature ratio and/or the ratio of the downstream electron temperature to the incident ion energy is crucial for understanding physics of SNR shocks. Electron heating is one of the central issues of collisionless shock (CS) physics. The heating mechanism is not completely clear until now. Heating due to random wave-particle interaction inside the shock front, which was adopted before the 1980s, is being revived now as stochastic heating (Stasiewicz & Eliasson, 2023). Since the 1980s the cross-shock potential is considered responsible for the heating, either adiabatic, with magnetic moment conservation (Feldman et al., 1982; Hull et al., 2001; Schwartz et al., 1988), or non-adiabatic, with electron demagnetization (Balikhin & Gedalin, 1994; Balikhin et al., 1993; Mozer & Sundkvist, 2013). In either case a substantial cross-shock potential jump occurs at the shock transition, decelerating ions and accelerating electrons from upstream toward downstream (Cohen et al., 2019; Dimmock et al., 2012; Hanson et al., 2019; Walker et al., 2004). High-resolution

electric field measurements by Magnetospheric Multiscale mission (MMS) revealed small-scale large-amplitude electric spikes inside the shock front (Kamaletdinov et al., 2022; Mozer & Sundkvist, 2013; See et al., 2013; Vasko et al., 2020, 2018, 2022; Wang et al., 2020, Wilson et al., 2010; Wilson III et al., 2014). Thus, the electric field in the CS transition is highly non-uniform at the scales which break conservation of the magnetic moment. The integral of this electric field over the shock transition is the cross-shock potential. Combination of strong small-scale spikes and weak mean field seem to explain both the energy invested into electron heating and isotropy of the electron distributions (Gedalin, 2020).

The mentioned mechanisms refer to what happens at the scale of the shock width. Observations of electromagnetic emission from SNR shocks are unable to resolve these scales. The electron temperature, inferred at these shocks from X-ray measurements, is the temperature averaged over a large downstream region (Helder et al., 2011; Rakowski et al., 2003). This inferred temperature is one of major parameters used to make conclusions about the shock itself (Vink et al., 2015). In the absence of a complete theory of CS structure and particle energization in them, the only way to establish the dependence of electron heating on the shock parameters is to perform statistical analysis of the distribution of downstream electron temperatures well behind the shock transition of the Earth bow shock and assume that the high-Mach number tail of this distribution is relevant to SNR shocks. This is the objective of the present paper. The previous sets of shocks used for similar analysis included 66 terrestrial bow shock crossings and 19 interplanetary shocks with most Alvénic Mach numbers of about 5 (Schwartz et al., 1988) and 94 bow shocks at Saturn (Masters et al., 2011) with the highest Mach number of ∼150. Here we extend the analysis onto a much larger selection of shocks from the overall 2997 MMS1 shock crossings (Lalti et al., 2022) and Mach numbers up to ∼20.

2. Data Selection

The database of 2797 MMS1 shock crossings in given on the SHARP webpage https://sharp.fmi.fi. The shocks were analyzed visually (Lalti et al., 2022). For each shock we used the magnetic field data in the survey mode (FGM-srvy) (Russell et al., 2016), eight samples/s. We used the ion and electron data in the fast mode (FPI-fast) (Pollock et al., 2016) with the time resolution 4.5 s. All the data was taken as Level 2 products provided by the MMS Science Data Center. For each shock crossing the magnetic field magnitude, the ion temperature, and the electron temperature were plotted in the interval ±1,200 s around the crossing time. For each shock the corresponding upstream and downstream regions were visually identified. The task imposes rather strict selection criteria, since we are not interested in electron temperatures either in the close vicinity of the transition region or in the downstream region where has not relaxed yet to a uniform state. Shocks, for which upstream or downstream regions could not be reliably determined, were rejected. Uniform downstream region may by not achieved if the magnetosheath width is insufficient for relaxation of large-amplitude magnetic oscillations. Upstream region cannot be reliably identified, for example, when a spacecraft crosses a shock from downstream to upstream and almost immediately crosses the shock again. MMS instruments often do not measure ion distributions reliably, and the electron moments (density and temperature) were used for most calculations. If the downstream parameters are determined in the truly uniform downstream region, the Rankine-Hugoniot relations (RH) limit the density and magnetic field ratios, $n_d/n_u \leq 4$ and $B_d/B_u \leq 4$. Here and hereafter the subscripts u and d refer to the upstream and downstream regions, respectively. If the measured B_d/B_u is slightly larger than four, it can be interpreted as an error of averaging due to magnetic oscillations. If the measured B_d/B_u is substantially larger than four, this indicates that a uniform downstream is not achieved. We therefore apply the selection criterion $B_d/B_u \leq 4.5$. In what follows we also exclude shocks with the Alfvénic Mach number larger than 25. The number of such shocks is very small and the dispersion of the parameters may be smaller than individual errors. The latter is difficult to estimate. This procedure left us with 517 selected shocks. Figure 1 shows two examples of "good" shocks included in the above mentioned selection. The explanation is in the figure caption. For comparison, Figure 2 shows two examples of the shocks excluded from the analysis. One of the main reasons for excluding shocks from the analysis was that the spacecraft did not spend sufficient time either in the upstream or in the downstream region, as in both examples in Figure 2. Our selection criteria do not disqualify time-dependent, rippled, or turbulent shocks, similar to those observed by Madanian et al. (2021) or simulated by Omidi et al. (2021). See, for example, Figure 1, right panel, where the shock front is not necessarily stationary nor planar. The only requirement is that the spacecraft reaches both upstream and downstream regions sufficiently far from the shock transition, so that we may reasonable assume that the distributions have already relaxed and there will not subsequent substantial changes.

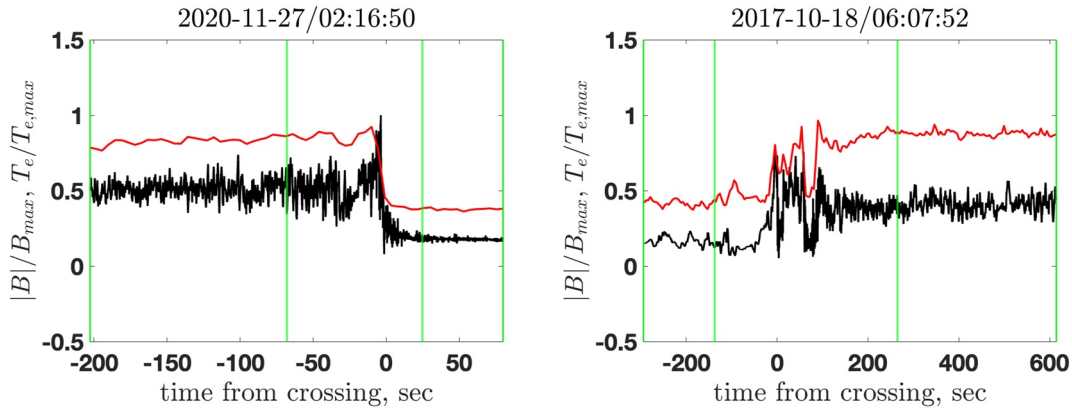

Figure 1. Examples of two shock crossings included in the selection for the analysis. The shock crossing is zero time. The magnetic field magnitude (black line) is normalized on the maximum magnetic field inside the window of ±1,200 s around the crossing. The electron temperature is normalized on the maximum temperature in the same window. The normalization is done to be able to put both variables in the same axes. The chosen upstream and downstream regions are delimited by the green lines. In both cases the upstream and downstream regions are sufficiently long and can be reliably identified. The level of the magnetic fluctuations in the downstream region is reasonably low so that determination of the downstream magnetic field is hopefully reliable too. The electron temperature seems to level off at uniform upstream and downstream values. Left panel: $\theta_{Bn} = 44°$, $M_A = 4.3$. Right panel: $\theta_{Bn} = 13°$, $M_A = 8.5$. See definitions in Section 3.

3. Analysis of the Selected Shocks

For each shock from the above selection we determined the shock speed and the Mach number M_A using the model shock normal $\hat{\boldsymbol{n}}$ (Farris & Russell, 1994), the measured upstream and downstream electron density n_{eu} and n_{ed}, the measured upstream and downstream electron bulk velocity vectors $\boldsymbol{V}_{eu}$ and $\boldsymbol{V}_{ed}$, and the upstream magnetic field vector $\boldsymbol{B}_u$. The shock parameters were calculated in the usual way:

$$V_u = \frac{(\boldsymbol{V}_{ed} - \boldsymbol{V}_{eu}) \cdot \hat{\boldsymbol{n}}}{1 - n_{eu}/n_{ed}} \tag{1}$$

$$v_A = \frac{B_u}{\sqrt{4\pi n_{eu} m_p}}, \qquad M_A = \frac{V_u}{v_A} \tag{2}$$

here v_A is the Alfvén speed, V_u is the upstream plasma velocity component along the shock normal in the shock frame, M_A is the Alfvénic Mach number, and m_p is the proton mass. The calculation assumes that the upstream proton and electron densities are equal, thus neglecting possible admixture of α-particles. The model shock normal (Farris & Russell, 1994) was used for the analysis and the angle between the shock normal $\hat{n}$ and the upstream magnetic field $\boldsymbol{B}_u$ is

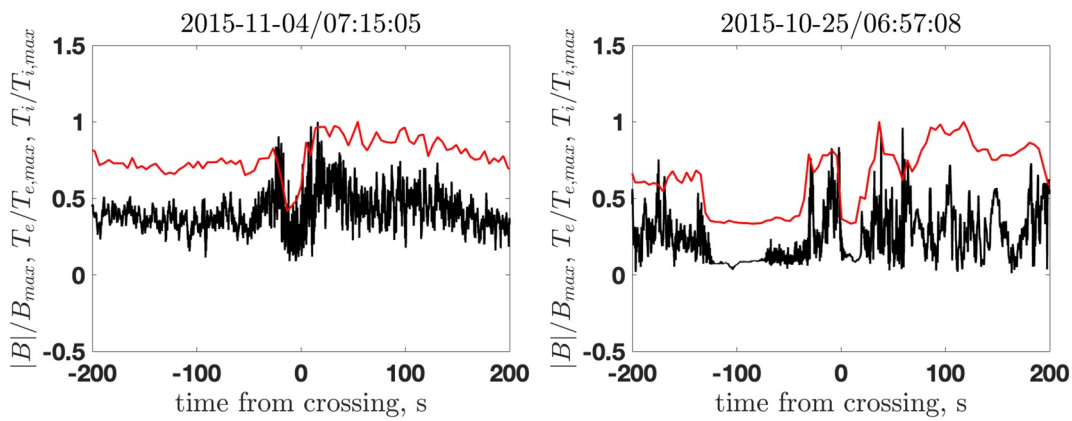

Figure 2. Examples of two crossings excluded from the analysis. The format is the same as in Figure 1.

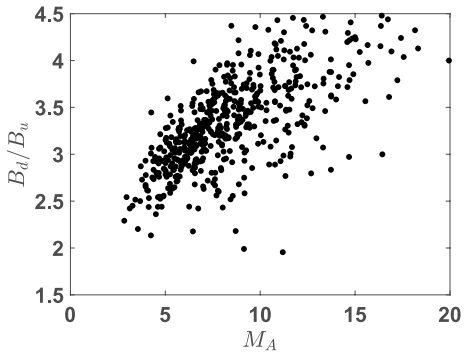

Figure 3. The Alfvénic Mach number M_A versus magnetic compression B_d/B_u.

$$\theta_{Bn} = \arccos\left|\frac{\hat{\boldsymbol{n}}\cdot\boldsymbol{B}_u}{B_u}\right| \quad (3)$$

If the upstream region is not properly resolved and the upstream magnetic field cannot be determined, even the knowledge of the model normal does not allow to determine θ_{Bn}. This alone reduced the number of useful shock crossings to 1,231.

For the fast Mach number calculation the fast magnetosonic speed v_F is needed, where

$$v_F^2 = \frac{1}{2}\left(v_A^2 + v_s^2 + \sqrt{\left(v_A^2 + v_s^2\right) - 4v_A^2 v_s^2 \cos^2\theta_{Bn}}\right) \quad (4)$$

This expression includes the sound speed $v_s^2 = \gamma(T_{eu} + T_{iu})/m_p$), where T_{eu} and T_{iu} are the upstream electron and ion temperatures, respectively, and γ is the adiabatic index which is usually assumed to be equal $\gamma = 5/3$. Given substantial uncertainties of the measurements of T_{iu}, the fast magnetosonic speed determination is much less reliable than the determination of the Alfvén speed. We therefore use here the Alfvénic Mach number and not the fast Mach number.

Figure 3 shows the magnetic compression B_d/B_u and density compression n_{ed}/n_{eu} as functions of M_A. The magnetic compression (right panel) behaves rather reasonably, increasing with increase of the Mach number and approaching $B_d/B_u \approx 4$ for $M_A > 10$. However, some of the values are still above the threshold, which, in most cases, indicates that large fluctuations of the downstream magnetic filed persist well behind the shock and affect the determination of the magnetic compression. These errors do not invalidate the analysis as long as there is sufficient dispersion in the distribution of the derived parameters and there is no systematic error.

Figure 4 shows the normalized downstream electron temperature $T_{ed}/\left(m_p V_u^2/2\right)$ (left panel) and the normalized heating $(T_{ed} - T_{eu})/\left(m_p V_u^2/2\right)$ as functions of the Alfvénic Mach number M_A. Here and hereafter the downstream temperature is the temperature averaged over the approximately uniform downstream region, sufficiently far from the overshoot, undershoot, and subsequent large amplitude oscillations, and where the temperature does not change much. The dispersion of the normalized temperatures is larger for lower M_A and becomes progressively smaller for higher Mach numbers. The normalized temperature seems to stabilize at 2%–5%. There is no indication of further decrease of $T_{ed}/\left(m_p V_u^2/2\right)$ for $M_A > 12$. The normalized heating seems to approach $(T_{ed} - T_{eu})/\left(m_p V_u^2/2\right) \approx (m_e/m_i)^{1/2}$ for large Mach numbers. This result is consistent with the earlier findings on the Saturn's bow shock (Masters et al., 2011).

The ratio of downstream electron-to-ion temperatures is shown in Figure 5. This ratio also stabilizes at $T_{ed}/T_{id} \approx 0.1$–$0.15$ for high Mach numbers.

The important question is whether electron heating depends strongly on the shock angle. Figure 6 shows histogram of $\cos\theta_{Bn}$ for the shocks for which the angle determination is possible and for the selected shocks. The distribution of $\cos\theta_{Bn}$ in the left panel (all shocks) corresponds to the expected random orientation of the magnetic field in the solar wind, which is supported by the earlier observations of the Earth bow shock by Cluster (Gedalin et al., 2021) and the observations of the interplanetary shocks by a number of spacecraft (Neugebauer, 2013). Most of the observed shocks are quasi-perpendicular shocks in all shock sets available so far. Only about 15% of all shocks have $\theta_{Bn} < 30°$. The selection procedure loses almost all these shocks. This reflects the difficulty of reliable identification of a uniform downstream for quasi-parallel shocks.

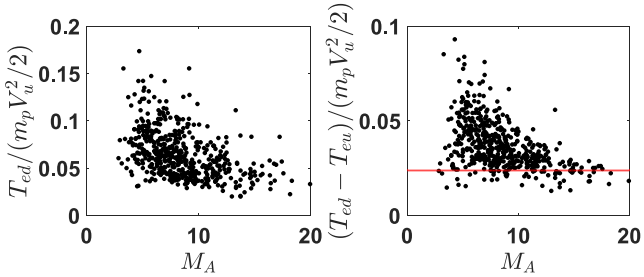

Figure 4. Left panel: the Alfvénic Mach number M_A versus the normalized downstream electron temperature $T_{ed}/\left(m_p V_u^2/2\right)$. Right panel: the Alfvénic Mach number M_A versus the normalized heating $(T_{ed} - Teu)/\left(m_p V_u^2/2\right)$. The horizontal red line corresponds to the ratio $\sqrt{m_e/m_i}$.

Figure 7 shows the dependence of the normalized downstream electron temperature $T_{ed}/\left(m_p V_u^2/2\right)$ on the shock angle θ_{Bn} (left panel) and also the distribution of the shock angles θ_{Bn} versus the Alfvénic Mach number M_A (right panel). There is no indication that heating at smaller angles differs significantly from heating at larger angles. If there is any difference it is too small to be interpreted as any dependence. On the other hand, higher Mach number shocks in the selection correspond to larger shock angles. Note that

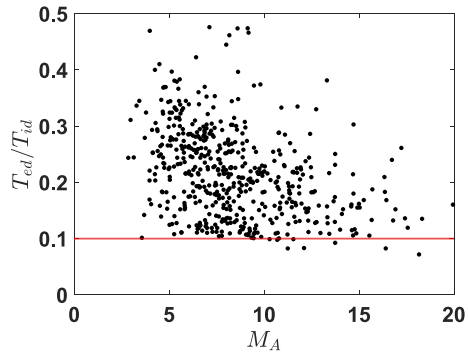

Figure 5. The Alfvénic Mach number M_A versus the ratio of the downstream temperatures T_{ed}/T_{id}. The red line is $T_{ed}/T_{id} = 0.1$.

we are interested in implications for SNR shocks and not in specific mechanisms of electron heating in shocks with different parameters. There is no reason to expect that θ_{Bn} are distributed completely differently in a SNR shock, and it is quite possible that the observed X-ray emission comes as a mixture from the sites with different θ_{Bn} at the global shock surface. Although electron heating might be different in quasi-parallel shocks, which are absent in the selection, it is difficult to expect that the trend in Figure 4 can be strongly effected, given that the fraction of such shock in the overall pool of the observed shocks is low.

One of the interesting observations is that electrons cool after the overshoot. Figure 8 shows the ratio of the maximum electron temperature to the downstream value. The maximum ratio $T_{e,\max}/T_{ed} \approx 1.5$ while typical $B_{\max}/B_d$ are noticeably larger. This should not be surprising since the magnetic field is measured with much higher resolution while the temperature is substantially averaged, which removes large fluctuations. This behavior of the electron temperature does not seem to be consistent with stochastic heating (Stasiewicz & Eliasson, 2023) unless there is also stochastic cooling. It might be consistent with the magnetic moment conservation with or without a smooth cross-shock potential (Feldman et al., 1982; Hull et al., 2001; Stasiewicz & Eliasson, 2023; Schwartz et al., 1988). However, this is not consistent with the isotropy of the electron distribution. Heating by a smooth cross-shock potential together with large-amplitude small-scale spikes of the electric field (Gedalin, 2020) is consistent with the temperature behavior and isotropy. This issue will be analyzed in depth elsewhere.

It was suggested that electron heating at the Earth bow shock may be nonlocal, because in the absence of Coulomb collisions electrons freely stream along the magnetic field line, which connects two sites with different parameters at the global shock surface, so that electron distributions produced at different shock mix (Mitchell & Schwartz, 2013). It has been shown recently (Kamaletdinov et al., 2022) that the small-scale electric fields in the shock front and around cause efficient pitch-angle diffusion of electrons in their phase space. The scattering on these small-scale fields plays the role of effective collisions, preventing electrons from freely streaming.

Finally, Figure 9 shows the dependence of $(T_{ed}/T_{eu})/(n_{ed}/n_{eu})^{2/3}$ on M_A. If the heating were adiabatic this ration would be equal to one (or close to it taking into account errors of measurements). The heating is clearly non-adiabatic.

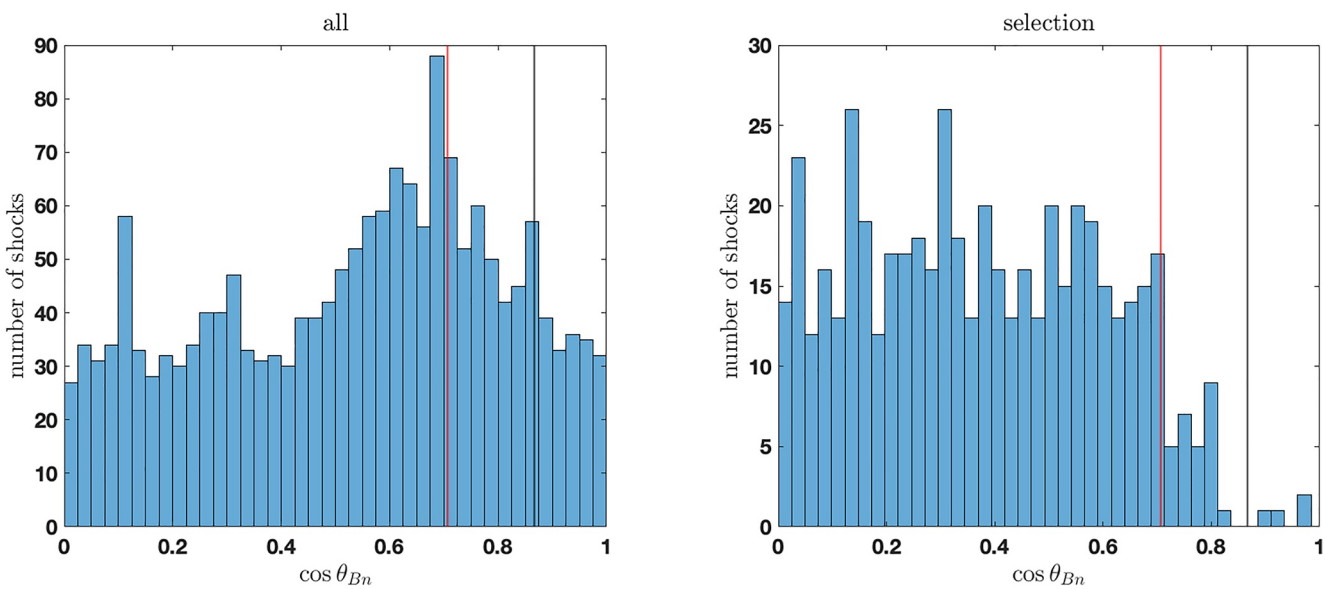

Figure 6. Left: distribution of $\cos\theta_{Bn}$ for the shocks for which the angle determination is possible. Right: distribution of $\cos\theta_{Bn}$ for the shocks in the selection. Red line corresponds to $\theta_{Bn} = 45°$, black lines shows $\theta_{Bn} = 30°$.

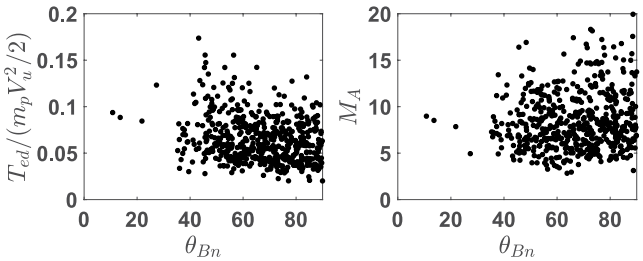

Figure 7. Left panel: the shock angle θ_{Bn} versus the normalized downstream electron temperature $T_{ed}/\left(m_pV_u^2/2\right)$. Right panel: the shock angle θ_{Bn} versus the Alfvénic Mach number M_A.

4. Conclusions

We have performed a statistical analysis of the dependence of the downstream electron temperatures on the Mach number. Of particular interest was the behavior of the ratios $T_{ed}/\left(m_pV_u^2/2\right)$ and T_{ed}/T_{id}. The first one describes the part of the incident ion energy transferred to electrons. The second one describes the relative efficiency of the electron and ion heating. Both ratios become approximately constant at large Mach numbers, $M_A \sim 20$. Neither becomes as small as m_e/m_p. It seems that $T_{ed}/\left(m_pV_u^2/2\right) \to 2-5\%$ while $T_{ed}/T_{id} \to 0.1$–0.15. The normalized heating $(T_{ed}-T_{eu})/\left(m_pV_u^2/2\right) \approx (m_e/m_i)^{1/2}$ for $M_A > 10$ probably hints on some universal mechanism of the conversion of the energy of the incident ions into electron heating, common for all high Mach number shocks.

In the above analysis the number or quasi-parallel shocks is small, because of the small number of shock quasi-parallel shock crossings and because of the selection criteria which exclude shocks with no well identified downstream region. It is not known what is the abundance of quasi-parallel shocks in nature. For a random direction of the magnetic field, like in the solar wind or interstellar medium, the number of quasi-parallel shocks is small, and it is difficult to expect that the overall emerging picture can be drastically changed if more quasi-parallel shocks were incorporated in the analysis. There is nothing in these arguments to exclude possible global arrangement of the magnetic field which favors the quasi-parallel geometry. The question of the contribution of quasi-parallel shocks in the statistics of the electron heating remains open until a sufficiently large set of such shocks becomes available for analysis of the downstream temperature of electrons. At present, electron heating is thought to be closely related to the cross-shock potential (Feldman et al., 1982; Schwartz et al., 1988), even if strong small-scale electric fluctuations are present (Gedalin, 2020). So far there are no indications that the mechanism of electron heating is different in quasi-perpendicular and quasi-parallel shocks. If it appears that electron heating in quasi-parallel shocks is substantially different this would raise the problem of explanation of why the cross-shock potential depends so strongly on the angle below $\theta_{Bn} \approx 30°$ or why the mechanism of heating changes abruptly. These issues are certainly worth studying but are beyond the scope of the present paper.

In the present analysis we limited ourselves with the Mach numbers $M_A \sim 20$. A smaller set of shocks with $M_A \sim 75$ has shown similar asymptotic behavior of $T_{ed}/\left(m_pV_u^2/2\right)$ (Masters et al., 2011). Unless the physical mechanism of electron heating changes drastically at $M_A \sim 100$, these above findings may be expected to be relevant for SNR shocks. If the heating keeps being determined by the cross-shock potential, this leads to another intriguing question: why the cross-shock potential becomes constant at very large Mach numbers?

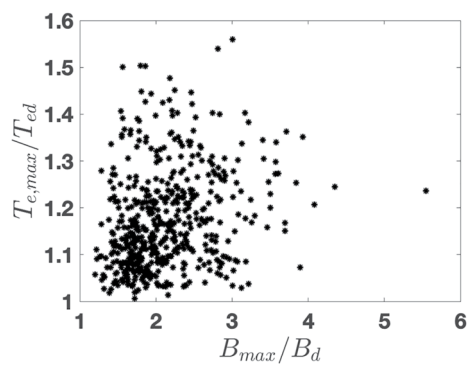

Figure 8. The normalized maximum magnetic field B_{max}/B_d versus the ratio of the maximum electron temperature to the downstream electron temperature $T_{e,max}/T_{ed}$.

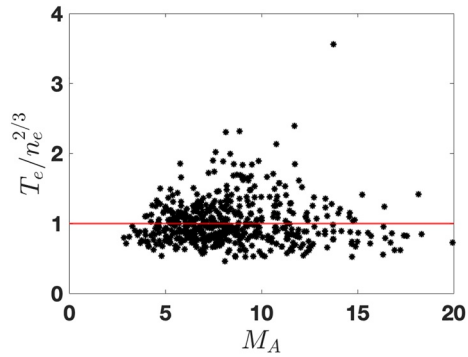

Figure 9. Dependence of $(T_{ed}/T_{eu})/(n_{ed}/n_{eu})^{2/3}$ on M_A. For adiabatic heating the points should lie on the horizontal red line.

Data Availability Statement

No new data sets were produced in the study. MMS data resides at the MMS Science Data Center https://lasp.colorado.edu/mms/sdc/public/.

Acknowledgments
The research was partially supported by the European Union's Horizon 2020 research and innovation program under grant agreement No 101004131 (SHARP).

References

Balikhin, M., & Gedalin, M. (1994). Kinematic mechanism of electron heating in shocks: Theory vs observations. *Geophysical Research Letters*, *21*(9), 841–844. https://doi.org/10.1029/94GL00371

Balikhin, M., Gedalin, M., & Petrukovich, A. (1993). New mechanism for electron heating in shocks. *Physical Review Letters*, *70*(9), 1259–1262. https://doi.org/10.1103/PhysRevLett.70.1259

Bell, A. R. (2004). Turbulent amplification of magnetic field and diffusive shock acceleration of cosmic rays. *MNRAS*, *353*(2), 550–558. https://doi.org/10.1111/mnr.2004.353.issue-2

Bell, A. R. (2005). The interaction of cosmic rays and magnetized plasma. *MNRAS*, *358*(1), 181–187. https://doi.org/10.1111/j.1365-2966.2005.08774.x

Cohen, I. J., Schwartz, S. J., Goodrich, K. A., Ahmadi, N., Ergun, R. E., Fuselier, S. A., et al. (2019). High-resolution measurements of the cross-shock potential, ion reflection, and electron heating at an interplanetary shock by MMS. *Journal of Geophysical Research*, *90*(A12), 3961–3978. https://doi.org/10.1029/2018JA026197

Dimmock, A. P., Balikhin, M. A., Krasnoselskikh, V. V., Walker, S. N., Bale, S. D., & Hobara, Y. (2012). A statistical study of the cross-shock electric potential at low Mach number, quasi-perpendicular bow shock crossings using Cluster data. *Journal of Geophysical Research*, *117*(A), 02210. https://doi.org/10.1029/2011JA017089

Farris, M. H., & Russell, C. T. (1994). Determining the standoff distance of the bow shock: Mach number dependence and use of models. *Journal of Geophysical Research*, *99*(A9), 17. https://doi.org/10.1029/94JA01020

Feldman, W., Bame, S., Gary, S., Gosling, J., McComas, D., Thomsen, M., et al. (1982). Electron heating within the Earth's bow shock. *Physical Review Letters*, *49*(3), 199–201. https://doi.org/10.1103/PhysRevLett.49.199

Gedalin, M. (2020). Large-scale versus small-scale fields in the shock front: Effect on the particle motion. *The Astrophysical Journal*, *895*(1), 59. https://doi.org/10.3847/1538-4357/ab8af0

Gedalin, M., Russell, C. T., & Dimmock, A. P. (2021). Shock mach number estimates using incomplete measurements. *Journal of Geophysical Research*, *126*(10), e2021JA029519. https://doi.org/10.1029/2021JA029519

Hanson, E. L. M., Agapitov, O. V., Mozer, F. S., Krasnoselskikh, V., Bale, S. D., Avanov, L., et al. (2019). Cross-shock potential in rippled versus planar quasi-perpendicular shocks observed by MMS. *Geophysical Research Letters*, *46*(5), 2381–2389. https://doi.org/10.1029/2018GL080240

Helder, E. A., Vink, J., & Bassa, C. G. (2011). Temperature equilibration behind the shock front: An optical and x-ray study of RCW 86. *The Astrophysical Journal*, *737*(2), 85. https://doi.org/10.1088/0004-637X/737/2/85

Hull, A. J., Scudder, J. D., Larson, D. E., & Lin, R. (2001). Electron heating and phase space signatures at supercritical, fast mode shocks. *Journal of Geophysical Research*, *106*(A8), 15711–15733. https://doi.org/10.1029/2001JA900001

Kamaletdinov, S. R., Vasko, I. Y., Artemyev, A. V., Wang, R., & Mozer, F. S. (2022). Quantifying electron scattering by electrostatic solitary waves in the Earth's bow shock. *Physics of Plasmas*, *29*(8), 082301. https://doi.org/10.1063/5.0097611

Lalti, A., Khotyaintsev, Y. V., Dimmock, A. P., Johlander, A., Graham, D. B., & Olshevsky, V. (2022). A database of MMS bow shock crossings compiled using machine learning. *Journal of Geophysical Research*, *127*(8), e2022JA030454. https://doi.org/10.1029/2022JA030454

Madanian, H., Desai, M. I., Schwartz, S. J., Wilson, L. B., Fuselier, S. A., Burch, J. L., et al. (2021). The dynamics of a high Mach number quasi-perpendicular shock: MMS observations. *The Astrophysical Journal*, *908*(1), 40. https://doi.org/10.3847/1538-4357/abcb88

Masters, A., Schwartz, S. J., Henley, E. M., Thomsen, M. F., Zieger, B., Coates, A. J., et al. (2011). Electron heating at Saturn's bow shock. *Journal of Geophysical Research*, *116*(A), A10107. https://doi.org/10.1029/2011JA016941

Mitchell, J. J., & Schwartz, S. J. (2013). Nonlocal electron heating at the Earth's bow shock and the role of the magnetically tangent point. *Journal of Geophysical Research*, *118*(12), 7566–7575. https://doi.org/10.1002/2013JA019226

Mozer, F. S., & Sundkvist, D. (2013). Electron demagnetization and heating in quasi-perpendicular shocks. *Journal of Geophysical Research*, *118*(9), 5415–5420. https://doi.org/10.1002/jgra.50534

Neugebauer, M. (2013). Propagating shocks. *Space Science Reviews*, *176*(1–4), 125–132. https://doi.org/10.1007/s11214-010-9707-2

Omidi, N., Desai, M., Russell, C. T., & Howes, G. G. (2021). High Mach number quasi-perpendicular shocks: Spatial versus temporal structure. *Journal of Geophysical Research*, *126*(9), e2021JA029287. https://doi.org/10.1029/2021JA029287

Pollock, C., Moore, T., Jacques, A., Burch, J., Gliese, U., Omoto, T., et al. (2016). Fast plasma investigation for magnetospheric multiscale. *Space Science Reviews*, *199*(1), 331–406. https://doi.org/10.1007/s11214-016-0245-4

Rakowski, C. E., Ghavamian, P., & Hughes, J. P. (2003). The physics of supernova remnant blast waves. II. Electron-ion equilibration in DEM L71 in the large magellanic cloud. *The Astrophysical Journal*, *590*(2), 846–857. https://doi.org/10.1086/375162

Russell, C. T., Anderson, B. J., Baumjohann, W., Bromund, K. R., Dearborn, D., Fischer, D., et al. (2016). The magnetospheric multiscale magnetometers. *Space Science Reviews*, *199*(1–4), 189–256. https://doi.org/10.1007/s11214-014-0057-3

Schwartz, S. J., Thomsen, M. F., Bame, S. J., & Stansberry, J. (1988). Electron heating and the potential jump across fast mode shocks. *Journal of Geophysical Research*, *93*(A11), 12923. https://doi.org/10.1029/JA093iA11p12923

See, V., Cameron, R. F., & Schwartz, S. J. (2013). Non-adiabatic electron behaviour due to short-scale electric field structures at collisionless shock waves. *Annales Geophysicae*, *31*(4), 639–646. https://doi.org/10.5194/angeo-31-639-2013

Stasiewicz, K., & Eliasson, B. (2023). Electron heating mechanisms at quasi-perpendicular shocks – Revisited with magnetospheric multiscale measurements. *MNRAS*, *520*(3), 3238–3244. https://doi.org/10.1093/mnras/stad361

Sulaiman, A. H., Masters, A., Dougherty, M. K., Burgess, D., Fujimoto, M., & Hospodarsky, G. B. (2015). Quasiperpendicular high Mach number shocks. *Physical Review Letters*, *115*(12), 125001. https://doi.org/10.1103/PhysRevLett.115.125001

Vasko, I. Y., Mozer, F. S., Bale, S. D., & Artemyev, A. V. (2022). Ion-acoustic waves in a quasi-perpendicular Earth's bow shock. *Geophysical Research Letters*, *49*(11), e2022GL098640. https://doi.org/10.1029/2022GL098640

Vasko, I. Y., Mozer, F. S., Krasnoselskikh, V. V., Artemyev, A. V., Agapitov, O. V., Bale, S. D., et al. (2018). Solitary waves across supercritical quasi-perpendicular shocks. *Geophysical Research Letters*, *45*(1), 5809–5817. https://doi.org/10.1029/2018GL077835

Vasko, I. Y., Wang, R., Mozer, F. S., Bale, S. D., & Artemyev, A. V. (2020). On the nature and origin of bipolar electrostatic structures in the Earth's bow shock. *Frontiers in Physics*, *8*, 156. https://doi.org/10.3389/fphy.2020.00156

Vink, J. (2020). *Physics and evolution of supernova remnants*. Springer International Publishing. https://doi.org/10.1007/978-3-030-55231-2

Vink, J., Broersen, S., Bykov, A., & Gabici, S. (2015). On the electron-ion temperature ratio established by collisionless shocks. *Astronomy and Astrophysics*, *579*, A13. https://doi.org/10.1051/0004-6361/201424612

Walker, S., Alleyne, H., Balikhin, M., André, M., & Horbury, T. (2004). Electric field scales at quasi-perpendicular shocks. *Annales Geophysicae*, *22*(7), 2291–2300. https://doi.org/10.5194/angeo-22-2291-2004

Wang, R., Vasko, I. Y., Mozer, F. S., Bale, S. D., Artemyev, A. V., Bonnell, J. W., et al. (2020). Electrostatic turbulence and Debye-scale structures in collisionless shocks. *The Astrophysical Journal Letters*, *889*(1), L9. https://doi.org/10.3847/2041-8213/ab6582

Wang, R., Vasko, I. Y., Mozer, F. S., Bale, S. D., Kuzichev, I. V., Artemyev, A. V., et al. (2021). Electrostatic solitary waves in the Earth's bow shock: Nature, properties, lifetimes, and origin. *Journal of Geophysical Research*, *126*(7), e2021JA029357. https://doi.org/10.1029/2021JA029357

Wilson, L. B., III, Sibeck, D. G., Breneman, A. W., Contel, O. L., Cully, C., Turner, D. L., et al. (2014). Quantified energy dissipation rates in the terrestrial bow shock: 2. Waves and dissipation. *Journal of Geophysical Research*, *119*(8), 6475–6495. https://doi.org/10.1002/2014JA019930

Wilson, L. B. I., Cattell, C. A., Kellogg, P. J., Goetz, K., Kersten, K., Kasper, J. C., et al. (2010). Large-amplitude electrostatic waves observed at a supercritical interplanetary shock. *Journal of Geophysical Research*, *115*(A), A12104. https://doi.org/10.1029/2010JA015332